Impact of chirality on the Glass Forming Ability and the crystallization from the amorphous state of 5-ethyl-5-methylhydantoin, a chiral poor glass former

Bienvenu Atawa, Nicolas Couvrat, Gérard Coquerel, Eric Dargent, Allisson Saiter-Fourcin

Impact of Chirality on the Glass Forming Ability and the Crystallization from the Amorphous State of 5-ethyl-5-methylhydantoin, a Chiral Poor Glass Former

Bienvenu Atawa, Nicolas Couvrat, Gérard Coquerel, Eric Dargent, Allisson Saiter

PII: S0378-5173(18)30070-X
DOI: https://doi.org/10.1016/j.ijpharm.2018.01.050
Reference: IJP 17293

To appear in: *International Journal of Pharmaceutics*

Received Date: 18 September 2017
Revised Date: 24 January 2018
Accepted Date: 25 January 2018

Please cite this article as: B. Atawa, N. Couvrat, G. Coquerel, E. Dargent, A. Saiter, Impact of Chirality on the Glass Forming Ability and the Crystallization from the Amorphous State of 5-ethyl-5-methylhydantoin, a Chiral Poor Glass Former, *International Journal of Pharmaceutics* (2018), doi: https://doi.org/10.1016/j.ijpharm.2018.01.050

Impact of Chirality on the Glass Forming Ability and the Crystallization from the Amorphous State of 5-ethyl-5-methylhydantoin, a Chiral Poor Glass Former

Bienvenu Atawa †§, Nicolas Couvrat §*, Gérard Coquerel §, Eric Dargent †, Allisson Saiter †*

† Normandie Univ, UNIROUEN Normandie, UMR CNRS 6634, Groupe de Physique des Matériaux, F76801 Saint Etienne du Rouvray

§ Normandie Univ, UNIROUEN Normandie, EA3233, Science et Méthodes Séparatives, F76821 Mont Saint Aignan, France

* Corresponding authors: nicolas.couvrat@univ-rouen.fr (+33 2 35 14 70 29); allison.saiter@univ-rouen.fr (+33 2 32 95 50 86)

Other authors: bienvenu.atawa@etu.univ-rouen.fr; gerard.coquerel@univ-rouen.fr; eric.dargent@univ-rouen.fr

Graphical Abstract

The Glassy state of a chiral molecular poor glass former (5-ethyl-5-methylhydantoin) was achieved by FSC while crystallization occurs by DSC. The glass transition temperature of the system (independent from the composition) was determined for the first time. The pure enantiomer presented a higher crystallization propensity compared to other compositions: crystallization of amorphous enantiopure material occurred 36 °C below Tg. Possible metastable equilibria (previously unknown) between both enantiomers were evidenced.

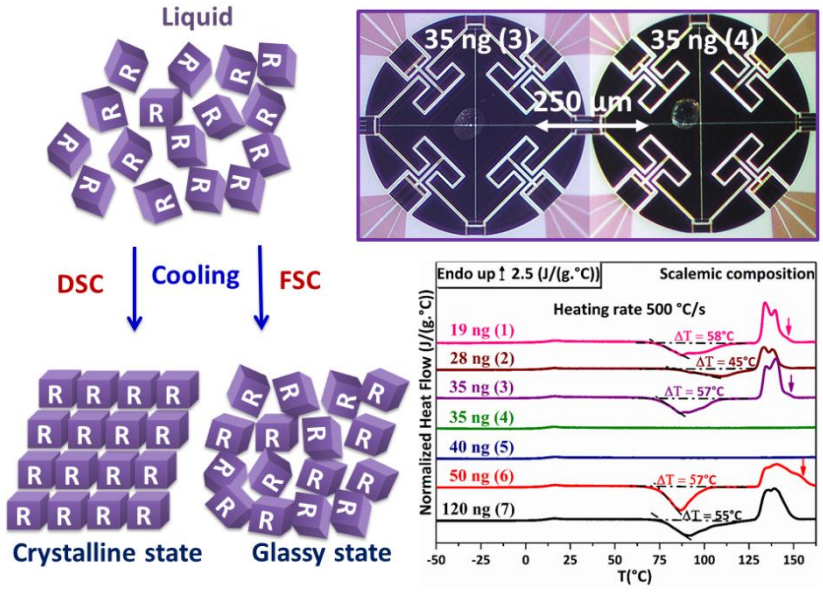

Abstract

The investigation of the glassy state of 5-ethyl-5-methylhydantoin (*i.e.* 12H, a chiral Active Pharmaceutical Ingredient) was attempted by Differential Scanning Calorimetry (DSC) and Fast Scanning Calorimetry (FSC). This compound exhibits a high crystallization propensity for every enantiomeric composition. Nevertheless, glassy states of pure enantiomer or mixtures between enantiomers were successfully reached by FSC at cooling rates of: 1000°C/s and 300 °C/s respectively, even though limitations on the sampling reproducibility were evidenced due to FSC sample size. The Glass Forming Ability (GFA) was proven to increase with the counter-enantiomer content. From the glassy state, pure enantiomer displayed a more pronounced crystallogenic character (with a crystallization occurring 36°C below Tg during ageing) than that of the mixture between enantiomers. Ageing of amorphous 12H promotes a strong nucleation behavior in both samples but enantiopure 12H crystallizes upon ageing while scalemic 12H evolves towards the metastable equilibrium. Finally, potential new phase equilibria (previously not reported) in the enantiomeric phase diagram could have been highlighted by FSC by recrystallization from the amorphous state.

Keywords

Fast Scanning Calorimetry, Glass Forming Ability, Chirality, Glassy state, Physical ageing

Chemical compounds studied in this article

5-Ethyl-5-methylhydantoin (PubChem CID: 82162)

Abbreviations

API: Active Pharmaceutical Ingredient

GFA: Glass Forming Ability

FSC: Fast Scanning Calorimetry

DSC: Differential Scanning Calorimetry

BCS: BioPharmaceutical Classification System

ee: Enantiomeric Excess

AS3PC: Auto-Seeded Programmed Polythermic Preferential Crystallization

1. Introduction

Active Pharmaceutical Ingredients (APIs) are mostly formulated in the crystalline state for obvious reasons of stability, chemical and structural purities (Variankaval *et al*., 2008). But regarding the Biopharmaceutical Classification System (BCS), not less than 90% of the commercialized APIs are poorly water soluble and consequently have poor bioavailability (Amidon *et al*., 1995). This fact is a critical issue for pharmaceutical industries. Many techniques are therefore proposed to enhance the bioavailability of APIs. Among them, the formulation of the APIs in the amorphous state is one of the most promising routes to enhance their bioavailabilities (Bhugra and Pikal, 2008; Hancock and Parks, 2000). Numerous operations may lead to amorphous compounds (Nagapudi and Jona, 2008; Vasconcelos *et al*., 2016): melt quenching, freeze and spray drying (Rey, 2016), high energy milling (Descamps *et al*., 2007; Schammé *et al*., 2016; Willart and Descamps, 2008), fast dehydration (Willart *et al*., 2002). If the targeted molecule is thermally stable at the liquid state, melt quenching remains one of the most common and easiest way to obtain pure amorphous material. Upon cooling, a liquid can either crystallize or remains liquid below the melting temperature. At a certain temperature, the super-cooled liquid falls in an out-of-equilibrium state (namely the glassy state) characterized by the glass transition temperature (Tg). At this temperature, the heat capacity, Cp of the super-cooled liquid decreases abruptly to a value slightly higher than that of the crystal (Descamps and Willart, 2016). This phenomenon has a kinetical character and is not a thermodynamic phase transition. Indeed, the higher the cooling rate, the higher the Tg value (Saiter *et al*., 2007). A shift of 3-5 °C can be observed as the cooling rate changes by one order of magnitude (Descamps and Willart, 2016).

Tg is considered as a reference temperature for the viability of an amorphous state and is intrinsic to the compound. Accordingly, its value can give some ideas about the storage temperature of an amorphous API. It also plays an important role during the phase transformation of a molecular compound submitted to mechanical or thermal solicitations such as milling. Indeed, applying the milling above or below Tg can respectively lead either to other molecular ordered phases (i.e. polymorphs) or to pure or partial amorphous materials (Descamps *et al.*, 2007), (Schammé *et al.*, 2016). Furthermore, the importance of Tg determination is well established for industrial drying processes such as freeze drying or spray drying. A porous amorphous solid, obtained by freeze drying may easily collapse or shrink if the storage temperature is above Tg (Bhandari and Howes, 1999). For all the above reasons, the determination of Tg is of a primary importance for pharmaceutical applications.

Differential scanning calorimetry (DSC) is one of the most conventional techniques used to evaluate Tg value for a given cooling or heating rate. Tg characterization is sometimes problematic for some molecular compounds: the glass transition region may overlap with different thermal events such as crystallization (Yu *et al.*, 1998) or structural enthalpy recovery, the heat capacity jump at the glass transition region can be of very small magnitude (Yu, 2001). Theoretically, crystallization can be avoided if sufficient cooling rate is provided (Debenedetti, 1996; Debenedetti and Stillinger, 2001; Turnbull, 1969). However, numerous molecular compounds exhibit a very high propensity to crystallize upon melt cooling, and standard DSC is limited in cooling rate ability (usually, an accurately cooling rate up to 50 °C/min). An alternative was proposed by High Performance DSC's (HPer) which improved the cooling maximum of more than 1 decade. The first HPer DSC was developed by Perkin Elmer and carries out scans up to 750 °C/min ("LAB SYS-DSC 8500-N5340501," n.d.). But still at these high cooling rates, it remains possible for some systems to regain the crystalline configuration. One of the most recent tools developed by Mettler Toledo is the Flash DSC (Fast Scanning

Calorimetry or FSC hereafter) device based on a calorimeter chip (Mathot *et al*., 2011; van Herwaarden *et al*., 2011; Zhuravlev and Schick, 2010a, 2010b) which can accurately provide very high cooling rates (up to 4000 °C/s) in a wide range of temperature and therefore could permit to avoid recrystallization of most highly crystallogenic systems. Furthermore, this technique has largely proven its worth in the investigation of disordered polymeric and metallic systems (Cangialosi et al., 2016; Dhotel et al., 2015; Gao et al., 2016; Monnier et al., 2017b, 2017a, 2017c; Schick and Androsch, 2016; Simon et al., 2016; Simon and Koh, 2016). Therefore, up to our knowledge, few studies are reported in the case of small organic molecular compounds (Corvis *et al*., 2015a, 2015b; Kawakami *et al*., 2012; Magoń *et al*., 2015; Schammé *et al*., 2017; Shamim *et al*., 2015).

The present work focuses on the case of 5-ethyl-5methyl-hydantoin (12H hereafter). This hydantoin derivative (Figure 1a) is used for its antibacterial and antifungal properties (Beilles *et al*., 2001) and is chiral. The racemic mixture (*i.e.* enantiomeric excess or ee=0%) crystallizes as a stable conglomerate (Beilles *et al*., 2001; Ndzié *et al*., 1999), which is an eutectic mixture (50/50 composition) between both enantiomers (ee=100%) with a simple eutectic melting as illustrated in Figure 1b. 12H exhibits a very high tendency to crystallize for both pure enantiomer and racemic composition, in such way that the amorphous state may not be obtained with conventional methods. This study aims thus at isolating amorphous states of enantiopure and racemic 12H, to determine their physical differences in terms of Glass Forming Ability (GFA) and crystallization propensity, and by extension to predict chirality implications on the glassy state of conglomerate forming systems.

"Figure 1"

2. Materials and methods

2.1 Materials

Racemic mixture of 12H was supplied by ABCR GmbH. The pure enantiomer was obtained by means of Auto-Seeded Programmed Polythermic Preferential Crystallization method (AS3PC) and performed by Beilles and co-workers (Beilles *et al.*, 2001). The melting temperatures measured in this work were T_m (R or S) = 173 ± 2°C for the pure enantiomer and T_m (RS) = 140 ± 2°C for the racemic composition, in accordance with the literature data (Ndzié *et al.*, 1999). The melting enthalpies were ΔH_m = 21 ±1 kJ/mol and ΔH_m = 18 ±1 kJ/mol for the pure enantiomer and racemic composition respectively.

2.2 Methods

2.2.1 DSC

The DSC experiments were launched with a Perkin Elmer 8500. This power controlled DSC is made of two independent identical small furnaces, one for the sample material and one for the reference. Cooling was ensured by a refrigerated cooling system (IntraCooler II, using a dual stage heat exchanger with the lowest puck temperature at -96°C), allowing a cooling down to -70°C. The baseline was calibrated in the range [-70°C; 200°C] at 10 °C/min (the same heating rate for all the experiments), the calibrations in temperature and enthalpy were achieved using indium and benzophenone as reference materials. Measurements were done under a nitrogen gas flow of 20 mL/min and the sample mass was about 5 mg. All the samples were submitted to a heat-cool-heat cyclic protocol at 10 °C/min for the heating and a cooling of 50 °C/min.

2.2.2 FSC

The measurements were performed with a power compensation twin-chip namely Flash DSC 1 (FSC) from Mettler-Toledo. The chip consists of two membranes (0.5 mm of diameter), one for the sample and the other one as the reference. There are 16 thermocouples (8 to control the temperature on the sample side and 8 to control the temperature on the reference side), symmetrically arranged around the sample and reference areas ensured temperature

measurements *(*Mathot *et al., 2011)*. Conditioning and correction of the chip were performed according to the manufacturer and prior to measurements. The cooling was ensured down to -70°C by an intracooler model Huber TC100. The Huber TC100 is a dual step cooling device that can ensure the cooling of the sensor down to -95°C. The sample was submitted to a nitrogen purge gas flow at a rate of 20 mL/min and placed on the sample chip area by the mean of an optical microscope and a long fiber for sample positioning.

Preparation of the sample: a first chip was used for the pure enantiomer and a second for the samples taken from the racemic batch. As detailed above, racemic 12H batch is composed by a 50/50 mixture of pure enantiomer crystals and so far, no racemic compound was characterized for this molecule. Therefore, despite a pre-milling (manually) of the powder to ensure homogenization, the experimental constraints on the sample size did not permit to isolate an equimolar proportion between enantiomers during the sampling from the racemic batch. Thus, the sampling from the racemic batch always led to samples at scalemic compositions (*i.e.* ee is different from 0% or 100%) and only the thermal signature of the samples could give an approximation of their enantiomeric compositions **(please refer to supplementary information for further details about sample composition variations)**.

Measurements: A first pre-melting step is launched to ensure a good thermal contact between the sample and the sensor. In this study, the samples were submitted to a heat-cool-heat cyclic protocol. The cooling and heating rates chosen were in the range [300 - 3000 °C/s]. The sample mass can be estimated by using an equivalence DSC- FSC based on the thermal properties of the liquid or the glassy state linked to the sample mass. These properties can be either the melting enthalpy or the heat capacity jump at the glass transition region (Schawe and Pogatscher, 2016). In this work, the sample mass used for FSC analyses was determined using Eq. 1:

$$\boldsymbol{m\,(FSC)} = \frac{\boldsymbol{\Delta H_m(FSC)}}{\boldsymbol{\Delta H_m(DSC)}} \times \boldsymbol{m\,(DSC)} \qquad \textbf{Eq. (1)}$$

where ΔH_m represents the area of the melting pic normalized by the cooling rate and m the sample mass.

2.2.3 Thermal lag considerations

In FSC analyses, the sample is directly deposited on the chip and is heated from the bottom part in contact with the chip. Hence, there could be a thermal gradient dependent from sample thermal conductivity and size (Schawe and Pogatscher, 2016). Dynamic and static temperature gradients linked to the sample size and the high scanning rate during FSC experiments are reported in literature (Schawe *et al.* 2015). The dynamic thermal lag at the glass transition is corrected by averaging Tg values on cooling and on heating. This dynamic thermal lag can be neglected for small organic compounds if three conditions are fulfilled: i) a good thermal contact is ensured between the sample and the sensor, ii) the sample thickness is lower than 10µm and iii) the heating rate is low enough (circa 1000 °C/s) (Schawe and Pogatscher, 2016). The static thermal gradient is essentially due to the temperature difference between the furnace and its immediate environment. This effect is mostly impacted by the sample thickness. As reported in the case of polystyrene (Schawe, 2015), the static thermal lag becomes obvious when the thickness of the sample is > 10 µm. Thickness calculation was purchased based on simple geometric considerations. We assume that the samples are 3D cylindrical objects with different geometrical bases. The sample volume can be determined knowing the density of the crystal lattice (d=1.28 g/cm^3) and the sample mass. Consequently knowing the area occupied by the sample on the chip, one can determine its thickness. A universal EPI-illuminator optical microscope equipped with a digital sight system camera from Nikon Corporation was used in reflection mode to observe the sample shape. Figure 2 depicts images of four samples of

different masses (from 19 to 120 ng) noted (a), (b), (c), (d) and table 1 summarizes the sample geometrical characteristics.

"Figure 2"

Table 1. Geometrical characteristics of samples (a), (b), (c) and (d)

Sample mass (ng)	Volume 10^1 (μm^3)	Surface (μm^2)	Thickness (μm)
(a) 19	**1484**	**2294**	**6.5**
(b) 35	**2734**	**3853**	**7.0**
(c) 50	**3906**	**8482**	**4.6**
(d) 120	**9375**	**10993**	**8.5**

In this study, all sample thicknesses were estimated below 10 µm and thermal lag effects were then considered as negligible (up to 120 ng of sample mass and a heating rate of 1500 °C/s).

3. Results

3.1 DSC

Figure 3 displays the thermal behavior of both pure enantiomer and racemic mixture upon heating and cooling (at 10 °C/min and 50 °C/min respectively). Upon heating, only a single thermal event corresponding to the melting of each compound is mentioned. Upon cooling, recrystallization was not inhibited despite the applied cooling rate. These observations support the highly crystallogenic character of this molecule. Other attempts to vitrify the liquid by applying higher cooling rates in the range [100 - 250] °C/min resulted in failure (data not shown here). Another possibility remained quenching directly (manually) the melt of both samples in liquid nitrogen. Nevertheless, this possibility was quickly put aside. Actually, during the quenching, an extremely fast crystal growth occurred leaving no chance for vitrification.

"Figure 3"

Considering that the glass formation probability increases when fast cooling is provided (Debenedetti, 1996; Debenedetti and Stillinger, 2001; Turnbull, 1969), vitrification and crystallization propensities of 12H were apprehended by FSC.

3.2 Pure enantiomer by FSC

Figure 4 illustrates the thermal signature of pure enantiomer upon cooling and the second heating by FSC. First, the recorded melting temperature was consistent with the value obtained by classical DSC (175°C). Thus, cooling rates higher than 500 °C/s were required to inhibit recrystallization and fully amorphize enantiopure 12H. The thermal signature of the glass transition was well illustrated by an endothermal step jump of the heat flow at Tg. The latter was measured on cooling and no obvious cooling rate dependency was noticed: $Tg_{(onset)}$ = 16 ± 2°C. Nevertheless, at cooling rates of 300 °C/s and 500 °C/s, partial crystallization was evidenced. Cold crystallization remained unavoidable when the compound was heated from the amorphous state, even at 3000 °C/s. Cold crystallization was always followed by an endothermal peak corresponding to the melting of enantiopure 12H.

"Figure 4"

In order to determine the temperature region where nucleation and growth maxima are located, a cyclic heat-cool protocol and annealing step at various temperatures well below and above Tg (from -50°C to 80°C) was applied. This thermal protocol consisted in cooling the melted sample at 1500 °C/s to an annealing temperature. The sample was kept for 30min at the annealing temperature and heated at 3000 °C/s up to 210 °C. As depicted in figure 5, no thermal event occurred upon heating when the annealing step was achieved from 70°C and beyond. For

isotherms performed in the range -10°C to 60°C, crystallization took place during the isotherm and upon heating, melting occurred at the pure enantiomer melting point. Annealing performed at -50°C and -30°C led to an overshoot peak at the glass transition region upon heating. Crystallization was evidenced in the range 75°C up to 130°C and melting at 173°C (enantiopure melting point). The nuclei formed at lower temperatures during the annealing and heating steps inevitably undergoes crystallization in the range 75°C up to 130°C. The crystal growth rate G (T) is apparently very high in this temperature domain. But the localization of the temperature region where nucleation rate N (T) is at its maximum is not obvious in this case. Whatever the annealing temperature (from Tg - 66°C up to Tg + 44°C), complete crystallization occurred during annealing or heating. Consequently the melting enthalpies obtained were almost similar. Indeed, nucleation takes place well below Tg up to Tg + 44°C. These results and their implications are discussed in section 4.3.

‘‘Figure 5’’

3.3 Scalemic Composition by FSC

Analyses were then carried out with samples coming from the racemic batch. As depicted in 2.3 section, the sampling limitations imposed by FSC prevented to analyze a real racemic sample but only a scalemic (intermediate) composition close to the racemic one. Figures 6a and 6b present the thermal signature of such 12H sample upon melt cooling and heating from the amorphous state respectively. Full vitrification of the melt was achieved upon cooling (even at 300 °C/s). $Tg_{(onset)}$ = 16 ± 2°C was determined from cooling measurements. Upon heating, cold crystallization appears (figure 6b) and the shape of the peak is highly heating rate dependent. The exothermic crystallization peak

was broadened and shifted towards higher temperatures as the heating rate increased. Furthermore, the crystallization enthalpy decreased as the heating rate increased. For heating rates lower than 3000 °C/s, the melting event was characterized as complex peak resulting from the overlapping of two successive endotherms. The first peak has an onset temperature around 130°C and the onset temperature of the second peak could be extrapolated to 135°C. At 3000 °C/s, only one endothermal peak was recorded with an onset temperature around 135°C.

"Figure 6"

As in the case of pure enantiomer, the identification of the temperature region where nucleation and crystal growth maxima are located was launch for the scalemic sample. The same cyclic melting-quenching to different annealing temperatures was applied for the same annealing time. This thermal protocol consisted in quenching at 1500 °C/s the melted sample at various annealing temperatures ranging from -50°C up to 90°C. The annealing step was launch for 30 min and the sample reheated at 3000 °C/s up to 175°C. Figure 7 presents the heating curves after the annealing process. No thermal event was mentioned when the sample was hold at Ta ≥70°C therefore no crystallization occurred during the annealing or the quenching-heating steps.

When 10°C ≤ Ta ≤ 50°C, the sample fully recrystallized during the annealing period and a single endothermal peak was evidenced at 128°C. Heating the annealed sample at 0°C, led to a well-defined exothermal peak from 60°C to 110°C followed by melting at 128°C with the same melting enthalpy as for the previous annealing temperatures. Nucleation occurs from Tg – 16°C up to Tg + 34°C and G (T) is especially high from 60°C up to 110°C.

When -50°C ≤ Ta ≤ -10°C, recrystallization was always evidenced in the range 90°C up to

125°C during the heating step. Accordingly, the maximum of growth rate G_1^{max} is localized in this temperature region. The recrystallized samples melt at 133°C and the crystallization enthalpy (as the melting enthalpy) increases as the annealing temperature increases. As the isothermal temperature increases from -50°C up to -10°C the number of nuclei formed during the annealing step increases. Therefore the maximum of nucleation rate N_1^{max} is approximatively located at Tg – 26°C. At the glass transition region an overshoot peak is mentioned synonym of an ageing effect.

"Figure 7"

Analyses were carried out with different samples of variable masses taken from the same racemic batch. The samples presented identical thermal signatures in the glass transition region and the same Tg values at a constant heating rate. As illustrated in figure 8, only the kinetical character of the glass transition was observed (a shift of 1 to 2°C) when the heating rate was increased from 500 °C/s up to 1000 °C/s or 1500 °C/s.

"Figure 8"

As depicted in 2.2.3 section, the thermal lag effect on Tg was considered as negligible for these experiments.

3.4 Physical ageing and crystallization propensity

A systematic study of physical ageing process was launch for pure enantiomer and scalemic composition. The melted sample was cooled down to -70°C at 1000 °C/s and heated 30°C above Tg in order to record the unaged glass signal. The sample was then cooled down to Ta (from

-40°C up to 5°C) and aged for 60 s (before the final heating step at 1000 °C/s up to 45°C, the sample is previously cooled down to -70°C). Figure 9 (a and b) presents the final heating curves after the ageing procedure for pure enantiomer and scalemic 12H respectively. Depending on the annealing temperature, a more or less intense overshoot peak occurs at the glass transition region. This behavior is due to the irreversible enthalpy recovery phenomenon and is classically observed for different glass formers (Cangialosi *et al*., 2013; Kovacs *et al*., 1963; Kozdras *et al*., 2011; Yoshioka *et al*., 1994) (Gunawan *et al*., 2006; Hancock *et al*., 1995; Surana *et al*., 2004). Figure 9 c depicts the enthalpy excess evolution as function of Ta. All the samples presented a bell shape enthalpy recovery curve with the same maximum at Tg – 28°C for an ageing time of 60s.

A significant drop of the heat capacity is observed in the case of pure enantiomer when the ageing is performed for 60 s at temperature higher than Tg – 21°C. The heat capacity drop in the case of the scalemic composition occurred when Ta was higher than Tg - 11°C for the same ageing time. This drop of heat capacity in the supercooled liquid point out the early stages of the crystallization.

“Figure 9. a, b,c ”

Moreover, for two selected ageing temperatures (Tg - 36°C and Tg - 26°C), ageing was performed for various ageing times ta, from 1s up to 14440s and 1s up to 900s respectively and according to the same thermal protocol. Enantiopure 12H crystallizes for the two ageing temperatures after short ageing time (see supplementary information: Glassy pure enantiomer). In contrary as illustrated in figure 10 a) in the case of scalemic 12H, the enthalpy

relaxation at the glass transition region increases as the ageing time increases up to a constant signal for longer ageing time. The overshoot peak increases with ageing time and reaches a constant magnitude more rapidly for Tg – 26°C than for Tg – 36°C. However at Tg – 36°C the overshoot area attained higher intensities. The out of equilibrium nature of the glassy state implies a slow evolution of the glass towards the metastable supercooled liquid state. Therefore, one can ask if the supercooled liquid equilibrium is reached when the saturation overshoot peak is obtained for the two ageing temperatures. To answer this question, two methods are usually proposed. The first method consists in comparing the excess of enthalpy at the supposed equilibrium and the value needed to reach the supercooled liquid state ($\Delta H_\infty = \Delta C_P$ (Ta - Tg)). The second method consists in calculating the fictive temperature Tf as function of the ageing time. Tf is defined as the actual temperature for the same compound in the equilibrium, metastable, supercooled state whose structure is expected to be similar to that of the non-equilibrium compound (Descamps and Willart, 2016). At the supercooled liquid equilibrium, the Tf value is equal to the ageing temperature. The calculation of ΔC_P only by FSC is problematic because of the uncertainty linked to the rough determination of the sample mass. Consequently in this analysis we chose to determine Tf evolution as function of the ageing time. The Tf is calculated from the heating curves using the ‘‘equal area rule’’ (Moynihan *et al*., 1976) method written here in terms of the heat flow:

$$\int_{T_f}^{T \gg T_g} (\dot{Q}_l - \dot{Q}_g)\, dT = \int_{T \ll T_g}^{T \gg T_g} (\dot{Q} - \dot{Q}_g)\, dT \qquad \textbf{Eq. (2)}$$

where $\dot{Q}_l$ and $\dot{Q}_g$ are the liquid and glassy heat flow lines and $\dot{Q}$ is the sample heat flow.

In Figure 10 c) the difference (Tf – Ta) is plotted as a function of the ageing time for the two ageing temperatures. The fictive temperature value reaches the ageing temperature after 120 s and 10800 s for Ta= Tg – 26°C and Ta= Tg – 36°C respectively. Thus the supercooled liquid state is reached for the the two ageing temperatures.

"Figure 10. a, b, c"

4. Discussion

4.1 High Crystallization propensity of 12H

As illustrated by DSC and FSC results, 12H exhibits a high crystallization propensity. This is a common feature shared by numerous small organic compounds (Baird *et al*., 2010). Due to their small size and relatively planar shape, the packing of such molecules in the crystalline configuration is mostly favored. It is well established that compounds with high molecular weight are difficult to crystallize compared to systems with low molecular weight (Baird *et al*., 2010). Moreover, the propensity to form a glass can be affected by the number of aromatic rings, number of electronegative atoms, presence of flexible and rotating branches, intermolecular and intramolecular connections (Baghel *et al*., 2016; Kawakami *et al*., 2015; Miyazaki *et al*., 2007). Furthermore, it was observed that liquids composed of symmetric molecules crystallize more easily than liquids made of asymmetric molecules. The case of meta and para xylene is commonly presented as an obvious example (Turnbull, 1969). The meta-xylene liquid can undergo cooling and vitrify, whereas for para-xylene isomer crystallization takes place in the same cooling conditions (Alba *et al*., 1990). The tendency to crystallize (or to vitrify reversibly) can be related to numerous parameters: dynamics (viscosity or molecular mobility), thermodynamics (the driven force of crystallization) (Baird *et al*., 2012; Gerges and Affouard, 2015), kinetics and structural (the complexity to rebuild the bond networks between molecules after melting) (Baird *et al*., 2012). None of these different parameters can be neglected when it comes to fully understand the GFA of a compound or its crystallization propensity.

Based on the presence or absence of crystallization upon a cyclic heat-cool-heat protocol, Baird and coworkers proposed a classification system established on a set of 51 molecular compounds (Baird *et al*., 2010). The set of molecules is classified into class I (class I (A), class I (B)), class II, and class III as a function of their GFA. From this classification, 12H (whatever the ee) could be considered as a class I (A) molecular compound, which means it would inevitably undergo crystallization upon moderate cooling (around 20 °C/min) or melt quenching in liquid N_2. As 12H system, class I molecules are usually of low molecular weight and present simple molecular structures with few flexible and rotating bonds (Baird *et al*., 2010). The structural resolution of enantiopure 12H has been reported previously by S. Beilles and co-authors (Beilles *et al*., 2001) and highlighted the presence of infinite H-bond chains along b-axis. These strong molecular ribbons (two H-bonds per molecule involving N1, O2 and N3, see figure 11) are held together by means of van der Walls contacts (Beilles *et al*., 2001), (Gervais *et al*., 2002). Moreover, the most probable flexible group (5-ethyl) is not implicated in the H-bond chain building. The crystallographic features of 12H match correctly with the previous ideas proposed by Baird and coworkers (Baird *et al* 2010).

"Figure 11"

4.2 Thermal lag and glass Transition

As presented above, the sample thickness was always < 10 µm in all experiments. Furthermore, in the same experimental conditions, Tg value remained constant when increasing the sample mass from 19 ng up to 120 ng. For these reasons, the thermal lag effects on Tg were neglected. Independently of the enantiomeric composition, $Tg_{(onset)}$ = 16±2 °C. Indeed, both enantiomers present the same scaler properties such as Tm, ΔH_m, Tg and ΔC_P. From Gordon Taylor Law reported in Eq. 3:

$$T_g(x) = \frac{xT_{gS}+(1-x)K\,T_{gR}}{x+(1-x)K}, \text{ where } K = \frac{\Delta C_{pR}}{\Delta C_{pS}} = 1 \qquad \textbf{Eq. (3)}$$

It was demonstrated that, $T_g(x) = T_{g\,S} = T_{g\,R} = T_{g\,RS}$ (Coquerel and Tamura, 2016). Many experimental confirmations have been reported in literature: limonene (Gallis *et al*., 2000), diprophylline (Viel *et al*., 2017) or ibuprofen (Kim *et al*., 2014). For the same cooling or heating conditions, Tg value was not impacted by the asymmetric property of chirality.

4.3 Impact of enantiomeric composition on GFA and crystallization propensity in the glassy state.

FSC results suggested that 500 °C/s was not fast enough to completely skip the crystallization process in the case of enantiopure 12H. From DSC data upon cooling, one can assess that the degree of supercooling of pure enantiomer was higher than that of racemic mixture but still, this parameter cannot explain why upon cooling the pure enantiomer presented a poor GFA compared to racemic mixture. Considering that crystallization conjugates nucleation and crystal growth stages (that are temperature dependent processes), there is a temperature range at which the rate of crystallization is maximum. Consequently, nucleation and crystal growth temperature dependency curves overlap in that region. The Nucleation rate N ($m^{-3}s^{-1}$) and crystal growth G ($m\ s^{-1}$) were high enough to produce supercritical nuclei and aggregation of the molecules (growth) respectively in such way that 500 °C/s was not fast enough to completely inhibit the crystallization of enantiopure 12H. By contrast, for the intermediate/scalemic compositions, crystallization was not evidenced upon cooling neither at 500 °C/s nor 300 °C/s. This fact highlights the role played by the counter enantiomer in the GFA of this conglomerate forming system. For numerous set of organic compounds (e.g. alkylamide derived from trans-1,2-bis(amino)cyclohexane, diprophylline), racemic mixture has a much higher propensity to crystallize compared to the enantiomeric counterpart (Coquerel and

Tamura, 2016; Viel *et al*., 2017). It is important to notice that the racemic mixtures studied in the mentioned works crystallize as racemic compounds (i.e. both enantiomers crystallize in the same crystal lattice) like more than 90% of racemic species (Coquerel and Tamura, 2016). By contrast, racemic 12H is a conglomerate forming system (around 5% of racemic mixtures). In our case the counter enantiomer acts like an impurity (of the same chemical nature) which delays or inhibits the crystallization process. Therefore, at intermediate enantiomeric compositions, 12H will have a higher GFA when compared to that of the pure enantiomer. If this counter-enantiomer effect is assumed in the whole composition domain of the binary system, GFA should then increase as the composition approaches the racemic mixture (ee decreases). From a structural point of view both systems are identical, the implication of the counter enantiomer could then be analyzed from a thermodynamic angle. The presence of the counter enantiomer modifies the molecular environment of the melt, which results in a modification of the thermodynamic and kinetics properties related to crystallization.

Similar observations may be considered when heating the amorphous glasses. Indeed, due to steric hindrance effects, the required time for molecules of one enantiomer in the supercooled liquid to regain their crystalline configurations will be increased as the sample contains the two opposite enantiomers. Independently from the fact that pure enantiomer has a poor GFA compared to the scalemic composition, the temperature region where crystallization takes place was shifted towards higher temperatures with the counter-enantiomer for the same scanning rate. Furthermore, nucleation and crystal growth domains of pure enantiomer overlap in a large temperature interval of about 70°C (from -10°C up to 60°C) while at the scalemic composition, the two processes can either be well separated or overlap in a temperature region of about 40°C (from 10°C up to 50°C) accordingly to the equilibrium reached after recrystallization. This is consistent with the higher GFA of the scalemic sample compared to that of the pure enantiomer.

Pure enantiomer was proven to crystallize after short ageing time at Tg – 36°C or Tg – 26°C **(See supplementary information: Glassy pure enantiomer)**. Even at this temperature range, where the structural bulk relaxation process is considered as frozen and only localized movements are expressed, enantiopure 12H had enough molecular mobility to regain the crystalline state. Moreover, the fact that nucleation and growth processes merge at low temperatures (Tg – 26°C) increases the probability for crystallization to occur well below Tg.

Nevertheless fast crystallization in the glassy state have been reported in literature for many molecular systems such as indomethacin (Wu and Yu, 2006), nifedipine (Zhu *et al*., 2008), griseofulvin (Yu, 2001), and ortho-terphenyl (Powell *et al*., 2015; Yu, 2016). This rapid crystallization process below Tg is usually attributed to the flimsy nature of the generated glassy material, which can easily promote crack formation (Descamps and Dudognon, 2014; Yu, 2016). Cracks can originate from deep quenching of the liquid for glass formation purposes (Powell *et al*., 2015; Willart *et al*., 2017). Fractures induce free surface that favored heterogeneous nucleation, consequently the activation barrier of nucleation, the interfacial energy and driving force of crystallization are lowered and rapid crystallization can therefore be facilitated at lower temperature (below Tg), (Descamps and Dudognon, 2014; Legrand *et al*., 1997; Willart *et al*., 2017). One important phenomenon that has also to be taken into account is the surface mobility that can help to amplify the process. It is well established that for many glassy molecular compounds the diffusion mechanism at the surface are higher than in the bulk for about 6 decades in magnitudes (Capaccioli *et al*., 2012; Powell *et al*., 2015; Yu, 2016; Zhu *et al*., 2010). Such cracks formation effects generating heterogeneous nucleation can be envisaged in enantiopure 12H.

By contrast to pure enantiomer behavior, the sample close to the racemic composition (scalemic sample) did not crystallize during the ageing process at the two ageing temperatures.

During the ageing process, scalemic sample evolves irreversibly towards the metastable equilibrium state. This evolution is induced by a progressive loss of free volume, enthalpy and entropy acquired during the initial step of glass formation. The intense overshoot peak registered originated from the recovery of the loosen properties upon heating. At temperature where molecular mobility is high enough, enthalpy recovery takes place (Descamps and Willart, 2016). For this reason, the temperature region where the structural relaxation appears is shifted towards higher temperature compared to an unaged glass. Enthalpy recovery depend on the pair (Ta, ta). As Ta evolves towards lower temperatures (highly deviate from Tg), molecular mobility in the glassy state becomes slower but the enthalpy and time needed to reach the supercooled liquid metastable equilibrium are greater. Accordingly, when Ta is close to Tg, equilibrium can be reached for short ageing time and enthalpy recovery magnitude is low. Indeed, to reach equilibrium, short annealing is insufficient when Ta deviates far from Tg. Therefore, enthalpy recovery intensity can also be low.

The equilibrium state (crystalline state) reached by enantiopure 12H after the ageing process is therefore physically different from the expected state (supercooled liquid state) reached by the scalemic sample. This evidenced the potential role played by chirality during the evolution from an out of equilibrium state towards equilibrium (stable or metastable) in such binary eutectic systems without detectable partial solid solution. The Scalemic sample aged at Tg – 26°C and Tg – 36°C reaches the metastable liquid state after 120s and 10800s. This is confirmed by the fact that Ta and Tf values are equal after 120s and 10800s for Ta= Tg – 26°C and Ta= Tg – 36°C respectively. Furthermore the enthalpy excess values are very intense almost 9 J/g for Ta= -10°C and 12.5 J/g for Ta= -20°C. This behavior is quite surprising considering that at this temperature range molecular mobility is very low and the metastable liquid state is rarely reached. Nevertheless, even after short ageing time (60 s) high enthalpy recovery values (7.5 J/g) are obtained for Ta around Tg - 28°C. Strangely, at this temperature range a maximum of

nucleation is reported for scalemic 12H. Ageing of amorphous 12H therefore simultaneously produces a strong nucleation behavior and an intriguing intense overshoot peak. The conjugation of these two previous events may bring to some relevant questions. One may ask about the critical nucleation size and the nature of such nucleation process at these low temperatures. The critical nucleation size must be extremely small. Under these conditions the reversion of a large part of the nuclei formed well below Tg can be expected at low temperature upon reheating. This effective melting could contribute to the intriguing large endothermic relaxation peak. Nonetheless, recent studies on physical ageing through FSC on amorphous polymeric systems have reported accelerated return towards equilibrium and high magnitude values of the overshoot peak during the ageing process (Koh et al., 2015, 2016; Monnier et al., 2017b; Simon and Koh, 2016). These effects are mostly due to the high cooling rate facilities provided by FSC and sample size. The initial glass formed upon high cooling rate possesses high enthalpy value and greater free volume compared to an amorphous glass formed by conventional DSC cooling rate facilities. High free volume is here required for an accelerated return towards the metastable equilibrium and high cooling rate provides this free volume during the early stages of glass formation.

The access to 12H amorphous states (only feasible by FSC) offered also new routes to isolate unknown crystalline phases. Indeed, annealing from Tg - 66°C up to Tg - 26°C and Tg - 16°C up to Tg + 44°C promoted the nucleation of two different crystalline forms with a melting point at 133°C ± 1°C and 128°C ± 1°C respectively. These equilibria obtained were not reported in the binary phase diagram between both enantiomers. Consequently, crystallization from the amorphous and supercooled liquid states may have revealed the existence of possible polymorphism, metastable racemic compound or metastable equilibria between the two enantiomers and this highlights the benefits of accessing to fleeting amorphous states by novel techniques such as FSC.

5. Conclusions

The investigation of the glassy state of 5-ethyl-5-methylhydantoin was successfully performed by FSC analyses. For the first time, the glassy state of 12H was reached, and its Tg value was determined: $Tg_{(onset)}$ = 16 ± 2 °C (cooling 1000 °C/s) regardless its enantiomeric composition.

Besides, this study revealed drastic limitations in the sampling procedure of Flash DSC device. Indeed, when dealing with physical mixtures, the overall composition could not be reproducibly maintained on the chip sensor. Other preparations or sampling routes (such as multiple dilutions of saturated solutions and evaporation of a droplet directly on the chip) should be envisaged to ensure defined compositions.

In the case of 12H, GFA was proven to be independent from the degree of undercooling. The poor GFA of 12H is related to the poor separation of the nucleation and crystal growth events in both pure enantiomer and scalemic composition. Nevertheless, FSC analyses highlighted that chirality clearly impacts GFA. Inversely from the behavior usually observed for racemic compounds, upon cooling, the pure enantiomer presented a higher crystallization propensity compared to the intermediate / scalemic composition. Therefore, samples containing both enantiomers could be easily vitrified compared to pure enantiomers. Upon heating, the counter-enantiomer acted like an impurity that delayed or inhibited recrystallization from the glassy state. In addition, the stability of the glasses was investigated by an ageing process. For the same ageing conditions, the initial glass formed evolves toward different equilibria. Ageing promotes a strong nucleation behavior in every sample and either crystallization or highly intense overshoot peak. When glassy pure enantiomer crystallizes during the ageing step, amorphous scalemic 12H evolves towards the metastable liquid equilibrium. A possible

explanation involving cracks formation in the trigger of heterogeneous nucleation and fast surface crystallization was proposed in the case of enantiopure 12H.

Furthermore, different putative metastable equilibria around 130°C and 135°C previously unknown from the binary phase diagram between both enantiomers have been highlighted. In particular, a metastable racemic compound may have recrystallized from the amorphous state but accurate tools such Second Harmonic Generation microscopy (to assess or not the centrosymmetry) would be required to confirm this hypothesis.

This study confirmed the large benefits brought by FSC to investigate molecular amorphous states (even with highly crystallogenic molecules) but also the limitations of the technique to investigate properly phase diagrams and metastable equilibria. The direct coupling between FSC and "classical" experimental techniques such as Secondary-Harmonic generation imaging Microscopy, Polarized Optical Microscopy, Temperature Resolved X-ray Diffraction would be interesting to draw a comprehensive view of the different equilibria (stable and metastable) in this binary chiral system.

Author Contributions

The manuscript was written through contributions of all authors. All authors have given approval to the final version of the manuscript.

Notes

The authors declare no competing financial interest.

Acknowlegments

The authors are grateful to FEDER and Region Normandie for the financial support of this work through the FEDER MACHI project.

Supporting Information

Variations in compositions during sampling: FSC limitations. This material is available free of charge.

References

Alba, C., Busse, L.E., List, D.J., Angell, C.A., 1990. Thermodynamic aspects of the vitrification of toluene, and xylene isomers, and the fragility of liquid hydrocarbons. The Journal of Chemical Physics 92, 617–624. https://doi.org/10.1063/1.458411

Amidon, G.L., Lennernäs, H., Shah, V.P., Crison, J.R., 1995. A Theoretical Basis for a Biopharmaceutic Drug Classification: The Correlation of in Vitro Drug Product Dissolution and in Vivo Bioavailability. Pharm Res 12, 413–420. https://doi.org/10.1023/A:1016212804288

Baghel, S., Cathcart, H., Redington, W., O'Reilly, N.J., 2016. An investigation into the crystallization tendency/kinetics of amorphous active pharmaceutical ingredients: A case study with dipyridamole and cinnarizine. European Journal of Pharmaceutics and Biopharmaceutics 104, 59–71. https://doi.org/10.1016/j.ejpb.2016.04.017

Baird, J.A., Santiago-Quinonez, D., Rinaldi, C., Taylor, L.S., 2012. Role of Viscosity in Influencing the Glass-Forming Ability of Organic Molecules from the Undercooled Melt State. Pharm Res 29, 271–284. https://doi.org/10.1007/s11095-011-0540-4

Baird, J.A., Van Eerdenbrugh, B., Taylor, L.S., 2010. A classification system to assess the crystallization tendency of organic molecules from undercooled melts. J. Pharm. Sci. 99, 3787–3806. https://doi.org/10.1002/jps.22197

Beilles, S., Cardinael, P., Ndzié, E., Petit, S., Coquerel, G., 2001. Preferential crystallisation and comparative crystal growth study between pure enantiomer and racemic mixture of a chiral molecule: 5-ethyl-5-methylhydantoin. Chemical Engineering Science, Industrial Crystallisation 56, 2281–2294. https://doi.org/10.1016/S0009-2509(00)00442-5

Bhandari, B.R., Howes, T., 1999. Implication of glass transition for the drying and stability of dried foods. Journal of Food Engineering 40, 71–79. https://doi.org/10.1016/S0260-8774(99)00039-4

Bhugra, C., Pikal, M.J., 2008. Role of Thermodynamic, Molecular, and Kinetic Factors in Crystallization from the Amorphous State. Journal of Pharmaceutical Sciences 97, 1329–1349. https://doi.org/10.1002/jps.21138

Cangialosi, D., Alegría, A., Colmenero, J., 2016. Cooling Rate Dependent Glass Transition in Thin Polymer Films and in Bulk, in: Fast Scanning Calorimetry. Springer, Cham, pp. 403–431. https://doi.org/10.1007/978-3-319-31329-0_13

Cangialosi, D., Boucher, V.M., Alegría, A., Colmenero, J., 2013. Physical aging in polymers and polymer nanocomposites: recent results and open questions. Soft Matter 9, 8619–8630. https://doi.org/10.1039/C3SM51077H

Capaccioli, S., Ngai, K.L., Paluch, M., Prevosto, D., 2012. Mechanism of fast surface self-diffusion of an organic glass. Phys Rev E Stat Nonlin Soft Matter Phys 86, 051503. https://doi.org/10.1103/PhysRevE.86.051503

Coquerel, G., Tamura, R., 2016. "Enantiomeric Disorder" Pharmaceutically Oriented, in: Descamps, rc (Ed.), Disordered Pharmaceutical Materials. Wiley-VCH Verlag GmbH & Co. KGaA, pp. 135–160. https://doi.org/10.1002/9783527652693.ch5

Corvis, Y., Wurm, A., Schick, C., Espeau, P., 2015a. Vitreous State Characterization of Pharmaceutical Compounds Degrading upon Melting by Using Fast Scanning Calorimetry. J. Phys. Chem. B 119, 6848–6851. https://doi.org/10.1021/acs.jpcb.5b03041

Corvis, Y., Wurm, A., Schick, C., Espeau, P., 2015b. New menthol polymorphs identified by flash scanning calorimetry. CrystEngComm 17, 5357–5359. https://doi.org/10.1039/C5CE00697J

Debenedetti, P.G., 1996. Metastable Liquids: Concepts and Principles. Princeton University Press.

Debenedetti, P.G., Stillinger, F.H., 2001. Supercooled liquids and the glass transition. Nature 410, 259–267. https://doi.org/10.1038/35065704

Descamps, M., Dudognon, E., 2014. Crystallization from the amorphous state: nucleation-growth decoupling, polymorphism interplay, and the role of interfaces. J Pharm Sci 103, 2615–2628. https://doi.org/10.1002/jps.24016

Descamps, M., Willart, J.-F., 2016. Some Facets of Molecular Disorder in Crystalline and Amorphous Pharmaceuticals, in: Descamps, rc (Ed.), Disordered Pharmaceutical Materials. Wiley-VCH Verlag GmbH & Co. KGaA, pp. 1–56. https://doi.org/10.1002/9783527652693.ch1

Descamps, M., Willart, J.F., Dudognon, E., Caron, V., 2007. Transformation of Pharmaceutical Compounds upon Milling and Comilling: The Role of Tg. Journal of Pharmaceutical Sciences 96, 1398–1407. https://doi.org/10.1002/jps.20939

Dhotel, A., Rijal, B., Delbreilh, L., Dargent, E., Saiter, A., 2015. Combining Flash DSC, DSC and broadband dielectric spectroscopy to determine fragility. J Therm Anal Calorim 121, 453–461. https://doi.org/10.1007/s10973-015-4650-9

Gallis, H.E., Miltenburg, J.C. van, Oonk, H.A.J., 2000. Polymorphism of mixtures of enantiomers: A thermodynamic study of mixtures of D- and L-limonene. Phys. Chem. Chem. Phys. 2, 5619–5623. https://doi.org/10.1039/B005603K

Gao, Y., Zhao, B., Yang, B., Schick, C., 2016. Fast Scanning Calorimetry of Phase Transitions in Metals, in: Fast Scanning Calorimetry. Springer, Cham, pp. 691–721. https://doi.org/10.1007/978-3-319-31329-0_21

Gerges, J., Affouard, F., 2015. Predictive Calculation of the Crystallization Tendency of Model Pharmaceuticals in the Supercooled State from Molecular Dynamics Simulations. J. Phys. Chem. B 119, 10768–10783. https://doi.org/10.1021/acs.jpcb.5b05557

Gervais, C., Beilles, S., Cardinaël, P., Petit, S., Coquerel, G., 2002. Oscillating Crystallization in Solution between (+)- and (−)-5-Ethyl-5-methylhydantoin under the Influence of Stirring. J. Phys. Chem. B 106, 646–652. https://doi.org/10.1021/jp012622s

Gunawan, L., Johari, G.P., Shanker, R.M., 2006. Structural Relaxation of Acetaminophen Glass. Pharm Res 23, 967–979. https://doi.org/10.1007/s11095-006-9898-0

Hancock, B.C., Parks, M., 2000. What is the True Solubility Advantage for Amorphous Pharmaceuticals? Pharm Res 17, 397–404. https://doi.org/10.1023/A:1007516718048

Hancock, B.C., Shamblin, S.L., Zografi, G., 1995. Molecular Mobility of Amorphous Pharmaceutical Solids Below Their Glass Transition Temperatures. Pharm Res 12, 799–806. https://doi.org/10.1023/A:1016292416526

Kawakami, K., Harada, T., Yoshihashi, Y., Yonemochi, E., Terada, K., Moriyama, H., 2015. Correlation between Glass-Forming Ability and Fragility of Pharmaceutical Compounds. J. Phys. Chem. B 119, 4873–4880. https://doi.org/10.1021/jp509646z

Kawakami, K., Usui, T., Hattori, M., 2012. Understanding the glass-forming ability of active pharmaceutical ingredients for designing supersaturating dosage forms. J. Pharm. Sci. 101, 3239–3248. https://doi.org/10.1002/jps.23166

Kim, T.H., Shibata, T., Kojima, S., Shin, D.-M., Hwang, Y.-H., Ko, J.-H., 2014. Comparison of thermal and elastic properties of glassy racemic and enantiomorphic ibuprofen studied by Brillouin light scattering and modulated differential scanning calorimetry. Current Applied Physics 14, 965–969. https://doi.org/10.1016/j.cap.2014.05.001

Koh, Y.P., Gao, S., Simon, S.L., 2016. Structural recovery of a single polystyrene thin film using Flash DSC at low aging temperatures. Polymer 96, 182–187. https://doi.org/10.1016/j.polymer.2016.04.047

Koh, Y.P., Grassia, L., Simon, S.L., 2015. Structural recovery of a single polystyrene thin film using nanocalorimetry to extend the aging time and temperature range. Thermochimica Acta, Chip Calorimetry 603, 135–141. https://doi.org/10.1016/j.tca.2014.08.025

Kovacs, A.J., Stratton, R.A., Ferry, J.D., 1963. DYNAMIC MECHANICAL PROPERTIES OF POLYVINYL ACETATE IN SHEAR IN THE GLASS TRANSITION TEMPERATURE RANGE. J. Phys. Chem. 67, 152–161. https://doi.org/10.1021/j100795a037

Kozdras, A., Golovchak, R., Shpotyuk, O., Szymura, S., Saiter, A., Saiter, J.-M., 2011. Light-assisted physical aging in chalcogenide glasses: Dependence on the wavelength of incident photons. Journal of Materials Research 26, 2420–2427. https://doi.org/10.1557/jmr.2011.264

LAB SYS-DSC 8500-N5340501 [WWW Document], n.d. . PerkinElmer. URL http://www.perkinelmer.com/product/dsc-8500-lab-system-n5340501 (accessed 7.6.17).

Legrand, V., Descamps, M., Alba-Simionesco, C., 1997. Glass-forming meta-toluidine: A thermal and structural analysis of its crystalline polymorphism and devitrification. Thermochimica Acta 307, 77–83. https://doi.org/10.1016/S0040-6031(97)00271-2

Magoń, A., Wurm, A., Schick, C., Pangloli, P., Zivanovic, S., Skotnicki, M., Pyda, M., 2015. Reprint of "Heat capacity and transition behavior of sucrose by standard, fast scanning and temperature-modulated calorimetry." Thermochimica Acta, Chip Calorimetry 603, 149–161. https://doi.org/10.1016/j.tca.2014.12.013

Mathot, V., Pyda, M., Pijpers, T., Vanden Poel, G., van de Kerkhof, E., van Herwaarden, S., van Herwaarden, F., Leenaers, A., 2011. The Flash DSC 1, a power compensation twin-type, chip-based fast scanning calorimeter (FSC): First findings on polymers. Thermochimica Acta, Special Issue: Interplay between Nucleation, Crystallization, and the Glass Transition 522, 36–45. https://doi.org/10.1016/j.tca.2011.02.031

Miyazaki, T., Yoshioka, S., Aso, Y., Kawanishi, T., 2007. Crystallization rate of amorphous nifedipine analogues unrelated to the glass transition temperature. International Journal of Pharmaceutics 336, 191–195. https://doi.org/10.1016/j.ijpharm.2006.11.052

Monnier, X., Maigret, J.-E., Lourdin, D., Saiter, A., 2017a. Glass transition of anhydrous starch by fast scanning calorimetry. Carbohydrate Polymers 173, 77–83. https://doi.org/10.1016/j.carbpol.2017.05.042

Monnier, X., Saiter, A., Dargent, E., 2017b. Physical aging in PLA through standard DSC and fast scanning calorimetry investigations. Thermochimica Acta 648, 13–22. https://doi.org/10.1016/j.tca.2016.12.006

Monnier, X., Saiter, A., Dargent, E., 2017c. Vitrification of PLA by fast scanning calorimetry: Towards unique glass above critical cooling rate? Thermochimica Acta 658, 47–54. https://doi.org/10.1016/j.tca.2017.10.019

Moynihan, C.T., Macedo, P.B., Montrose, C.J., Montrose, C.J., Gupta, P.K., DeBolt, M.A., Dill, J.F., Dom, B.E., Drake, P.W., Easteal, A.J., Elterman, P.B., Moeller, R.P., Sasabe, H., Wilder, J.A., 1976. Structural Relaxation in Vitreous Materials*. Annals of the New York Academy of Sciences 279, 15–35. https://doi.org/10.1111/j.1749-6632.1976.tb39688.x

Nagapudi, K., Jona, J., 2008. Amorphous Active Pharmaceutical Ingredients in Preclinical Studies: Preparation, Characterization, and Formulation. Current Bioactive Compounds 4, 213–224. https://doi.org/10.2174/157340708786847852

Ndzié, E., Cardinael, P., Petit, M.N., Coquerel, G., 1999. Enantiomeric resolution of (+/-)-5-ethyl-5-methylhydantoin by means of preferential nucleation. Enantiomer 4, 97–+.

Powell, C.T., Xi, H., Sun, Y., Gunn, E., Chen, Y., Ediger, M.D., Yu, L., 2015. Fast Crystal Growth in o-Terphenyl Glasses: A Possible Role for Fracture and Surface Mobility. J. Phys. Chem. B 119, 10124–10130. https://doi.org/10.1021/acs.jpcb.5b05389

Rey, L., 2016. Freeze-Drying/Lyophilization of Pharmaceutical and Biological Products, Third Edition. CRC Press.

Saiter, A., Couderc, H., Grenet, J., 2007. Characterisation of structural relaxation phenomena in polymeric materials from thermal analysis investigations. Journal of Thermal Analysis and Calorimetry 88, 483–488. https://doi.org/10.1007/s10973-006-8117-x

Schammé, B., Couvrat, N., Malpeli, P., Dudognon, E., Delbreilh, L., Dupray, V., Dargent, E., Coquerel, G., 2016. Transformation of an active pharmaceutical ingredient upon high-energy milling: A

process-induced disorder in Biclotymol. International Journal of Pharmaceutics 499, 67–73. https://doi.org/10.1016/j.ijpharm.2015.12.032

Schammé, B., Monnier, X., Couvrat, N., Delbreilh, L., Dupray, V., Dargent, E., Coquerel, G., 2017. Insights on the Physical State Reached by an Active Pharmaceutical Ingredient upon High-Energy Milling. J. Phys. Chem. B 121, 5142–5150. https://doi.org/10.1021/acs.jpcb.7b02247

Schawe, J.E.K., 2015. Measurement of the thermal glass transition of polystyrene in a cooling rate range of more than six decades. Thermochimica Acta, Chip Calorimetry 603, 128–134. https://doi.org/10.1016/j.tca.2014.05.025

Schawe, J.E.K., Pogatscher, S., 2016. Material Characterization by Fast Scanning Calorimetry: Practice and Applications, in: Schick, C., Mathot, V. (Eds.), Fast Scanning Calorimetry. Springer International Publishing, pp. 3–80. https://doi.org/10.1007/978-3-319-31329-0_1

Schick, C., Androsch, R., 2016. New Insights into Polymer Crystallization by Fast Scanning Chip Calorimetry, in: Fast Scanning Calorimetry. Springer, Cham, pp. 463–535. https://doi.org/10.1007/978-3-319-31329-0_15

Shamim, N., Koh, Y.P., Simon, S.L., McKenna, G.B., 2015. The glass transition of trinitrotoluene (TNT) by flash DSC. Thermochimica Acta 620, 36–39. https://doi.org/10.1016/j.tca.2015.10.003

Simon, C., Zhang, Y., Wilde, G., 2016. Nucleation Kinetics Analyses of Deeply Undercooled Metallic Liquids by Fast Scanning Calorimetry, in: Fast Scanning Calorimetry. Springer, Cham, pp. 661–689. https://doi.org/10.1007/978-3-319-31329-0_20

Simon, S.L., Koh, Y.P., 2016. The Glass Transition and Structural Recovery Using Flash DSC, in: Fast Scanning Calorimetry. Springer, Cham, pp. 433–459. https://doi.org/10.1007/978-3-319-31329-0_14

Surana, R., Pyne, A., Suryanarayanan, R., 2004. Effect of Aging on the Physical Properties of Amorphous Trehalose. Pharm Res 21, 867–874. https://doi.org/10.1023/B:PHAM.0000026441.77567.75

Turnbull, D., 1969. Under what conditions can a glass be formed? Contemporary Physics 10, 473–488. https://doi.org/10.1080/00107516908204405

van Herwaarden, S., Iervolino, E., van Herwaarden, F., Wijffels, T., Leenaers, A., Mathot, V., 2011. Design, performance and analysis of thermal lag of the UFS1 twin-calorimeter chip for fast scanning calorimetry using the Mettler-Toledo Flash DSC 1. Thermochimica Acta, Special Issue: Interplay between Nucleation, Crystallization, and the Glass Transition 522, 46–52. https://doi.org/10.1016/j.tca.2011.05.025

Variankaval, N., Cote, A.S., Doherty, M.F., 2008. From form to function: Crystallization of active pharmaceutical ingredients. AIChE J. 54, 1682–1688. https://doi.org/10.1002/aic.11555

Vasconcelos, T., Marques, S., das Neves, J., Sarmento, B., 2016. Amorphous solid dispersions: Rational selection of a manufacturing process. Advanced Drug Delivery Reviews, Amorphous pharmaceutical solids 100, 85–101. https://doi.org/10.1016/j.addr.2016.01.012

Viel, Q., Brandel, C., Cartigny, Y., Eusébio, M.E.S., Canotilho, J., Dupray, V., Dargent, E., Coquerel, G., Petit, S., 2017. Crystallization from the Amorphous State of a Pharmaceutical Compound: Impact of Chirality and Chemical Purity. Crystal Growth & Design 17, 337–346. https://doi.org/10.1021/acs.cgd.6b01566

Willart, J.F., De Gusseme, A., Hemon, S., Descamps, M., Leveiller, F., Rameau, A., 2002. Vitrification and Polymorphism of Trehalose Induced by Dehydration of Trehalose Dihydrate. J. Phys. Chem. B 106, 3365–3370. https://doi.org/10.1021/jp012836+

Willart, J.F., Descamps, M., 2008. Solid State Amorphization of Pharmaceuticals. Mol. Pharmaceutics 5, 905–920. https://doi.org/10.1021/mp800092t

Willart, J.F., Dudognon, E., Mahieu, A., Eddleston, M., Jones, W., Descamps, M., 2017. The role of cracks in the crystal nucleation process of amorphous griseofulvin. Eur. Phys. J. Spec. Top. 226, 837–847. https://doi.org/10.1140/epjst/e2016-60358-y

Wu, T., Yu, L., 2006. Surface Crystallization of Indomethacin Below Tg. Pharm Res 23, 2350–2355. https://doi.org/10.1007/s11095-006-9023-4

Yoshioka, M., Hancock, B.C., Zografi, G., 1994. Crystallization of indomethacin from the amorphous state below and above its glass transition temperature. J. Pharm. Sci. 83, 1700–1705. https://doi.org/10.1002/jps.2600831211

Yu, L., 2016. Surface mobility of molecular glasses and its importance in physical stability. Advanced Drug Delivery Reviews, Amorphous pharmaceutical solids 100, 3–9. https://doi.org/10.1016/j.addr.2016.01.005

Yu, L., 2001. Amorphous pharmaceutical solids: preparation, characterization and stabilization. Advanced Drug Delivery Reviews, Characterization of the Solid State 48, 27–42. https://doi.org/10.1016/S0169-409X(01)00098-9

Yu, L., Mishra, D.S., Rigsbee, D.R., 1998. Determination of the Glass Properties of D-Mannitol Using Sorbitol as an Impurity. Journal of Pharmaceutical Sciences 87, 774–777. https://doi.org/10.1021/js970224o

Zhu, L., Jona, J., Nagapudi, K., Wu, T., 2010. Fast Surface Crystallization of Amorphous Griseofulvin Below Tg. Pharm Res 27, 1558–1567. https://doi.org/10.1007/s11095-010-0140-8

Zhu, L., Wong, L., Yu, L., 2008. Surface-Enhanced Crystallization of Amorphous Nifedipine. Mol. Pharmaceutics 5, 921–926. https://doi.org/10.1021/mp8000638

Zhuravlev, E., Schick, C., 2010a. Fast scanning power compensated differential scanning nano-calorimeter: 1. The device. Thermochimica Acta 505, 1–13. https://doi.org/10.1016/j.tca.2010.03.019

Zhuravlev, E., Schick, C., 2010b. Fast scanning power compensated differential scanning nano-calorimeter: 2. Heat capacity analysis. Thermochimica Acta 505, 14–21. https://doi.org/10.1016/j.tca.2010.03.020

Captions

Figure 1. a) Developed Formulae of racemic 12H, b) Binary phase diagram between 12H enantiomers

Figure 2. Pre-molten samples with different geometric parameters

Figure 3. Heating and cooling curves of pure enantiomer (left part) and racemic mixture (right part) in classical DSC

Figure 4. Thermal events of enantiopure 12H upon cooling (left part) and second heating (right part) at variable cooling and heating rates.

Figure 5. FSC scans of pure enantiomer recorded upon heating at 3000 °C/s after the melt cooled at different isothermal temperatures Ta (from -50 °C up to 80°C) and annealed for 30 min. N(T) and G(T) refers to nucleation and growth temperature region respectively.

Figure 6. a) Thermal events upon cooling and b) upon heating for the sample at a scalemic composition

Figure 7. FSC curves of scalemic 12H recorded upon heating at 3000 °C/s after the melt was cooled at different isothermal temperatures Ta (from -50 °C to 70°C) and annealed for 30 min. N(T) and G(T) refers to the temperature region where nucleation and growth take place respectively. N_1^{max} and G_1^{max} refers to the temperature region where the rate of nucleation and crystal growth are at their maxima.

Figure 8. Glass transition signature at 1000 °C/s and 1500 °C/s for three samples with increasing masses

Figure 9. a, b) FSC heating scans at 1000 °C/s as a function of ageing temperatures for an ageing time of 60s after cooling at 1000 °C/s for pure enantiomer and scalemic 12H respectively c)Evolution of the enthalpy excess value as a function of the difference (Ta – Tg)

Figure 10. a, b) FSC heating scans of scalemic 12H at 1000 °C/s as a function of ageing time for Ta= -20°C and -10°C respectively after cooling at 1000 °C/s c) Evolution of the difference (Tf – Ta) as a function of ageing time t_a.

Figure 11. Projection of the crystal structure of 12H along a-axis showing molecular ribbons running along the b-axis from C. Gervais et al (2002).

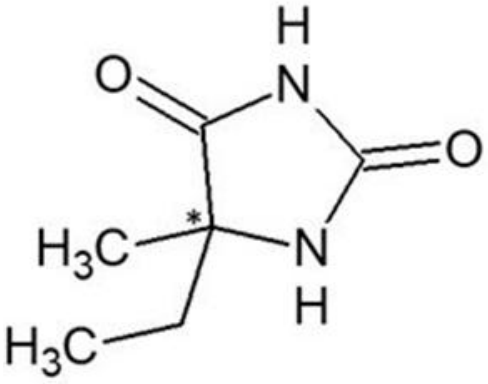

a)

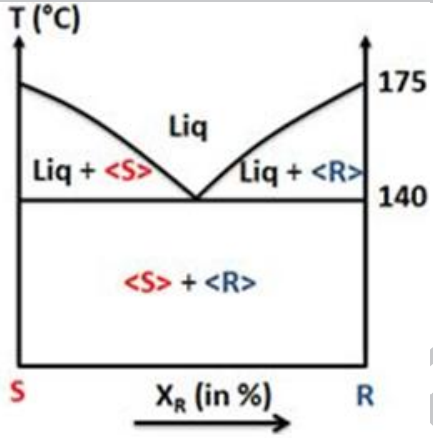

b)

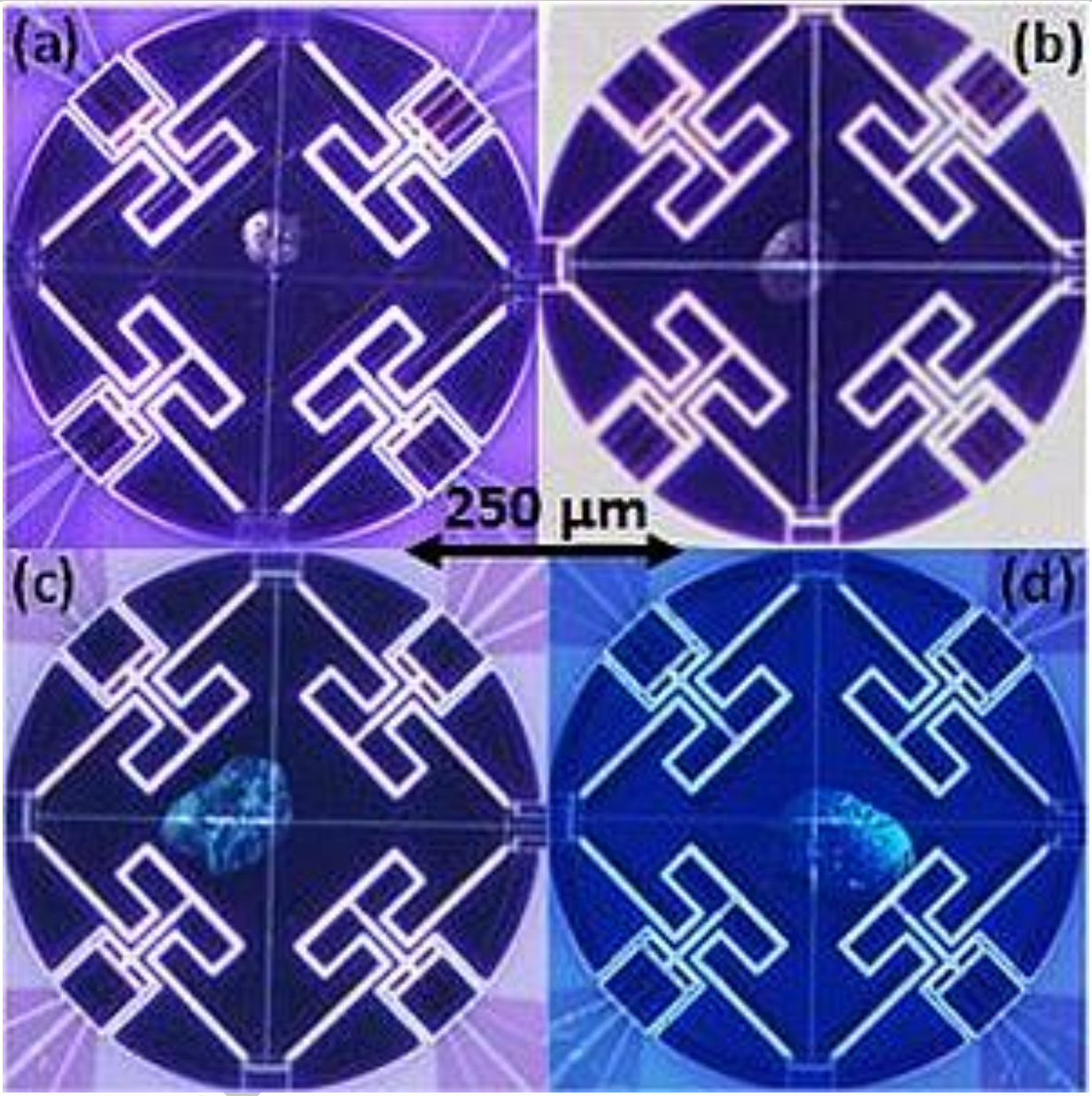

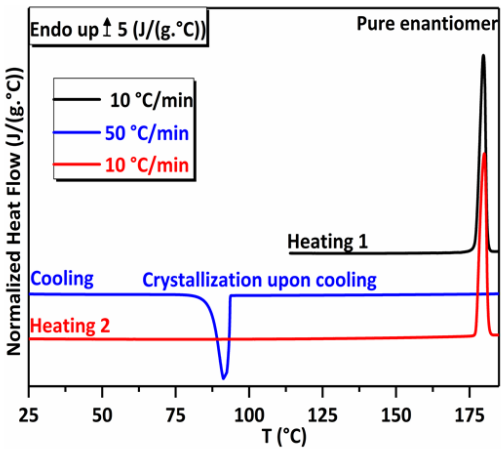

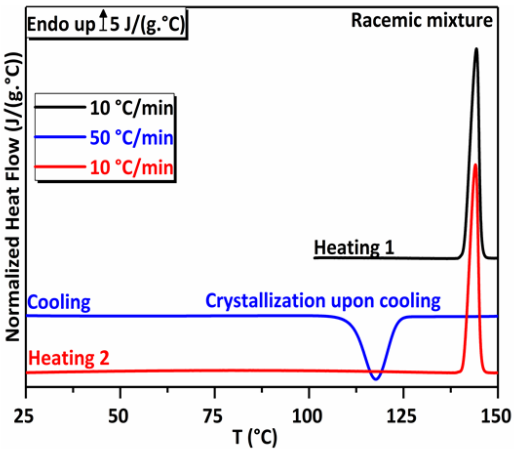

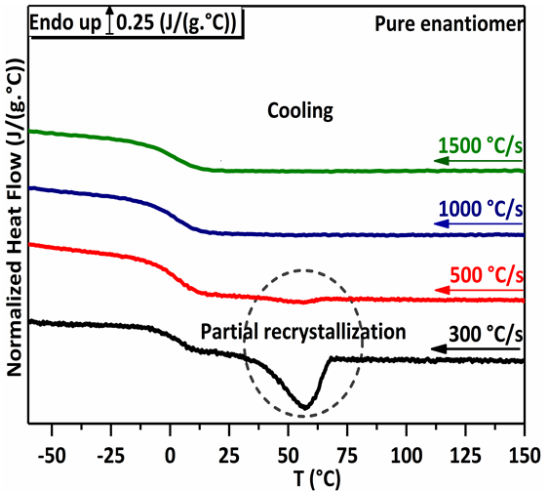

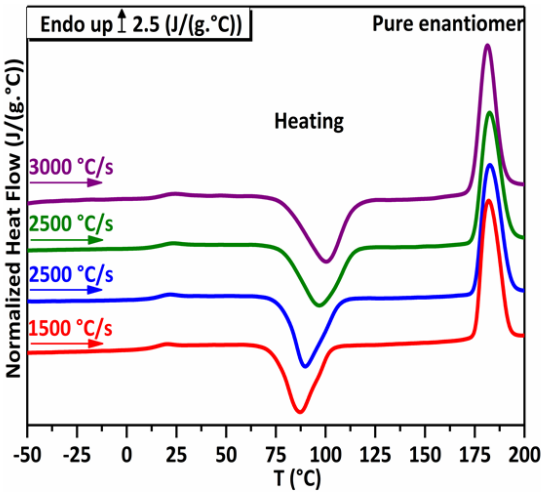

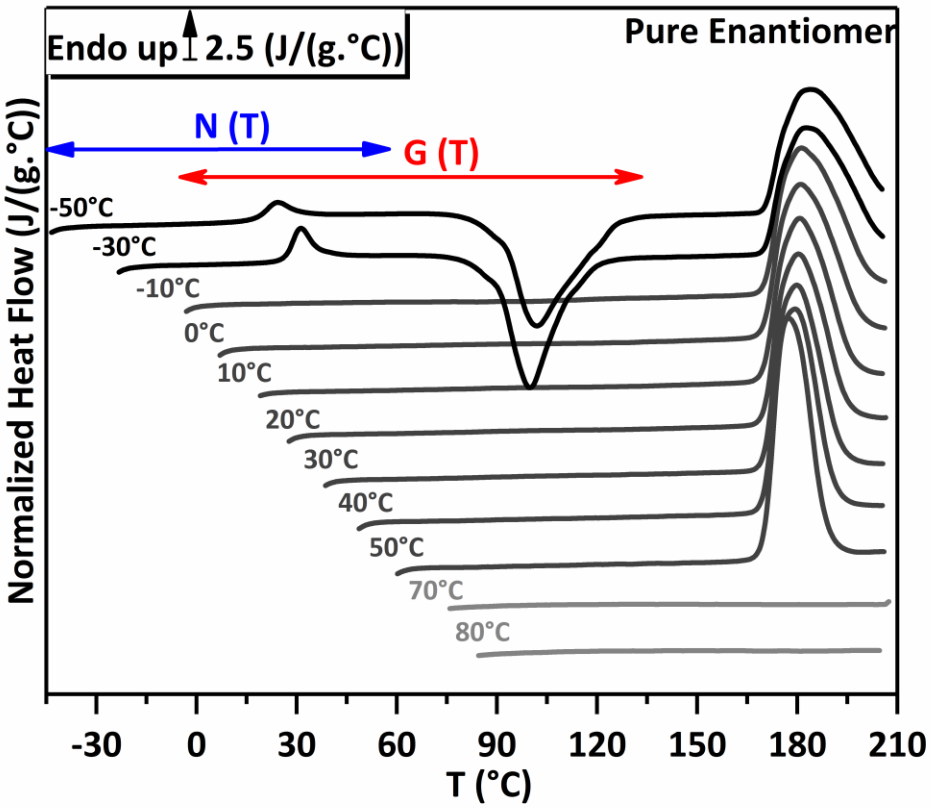

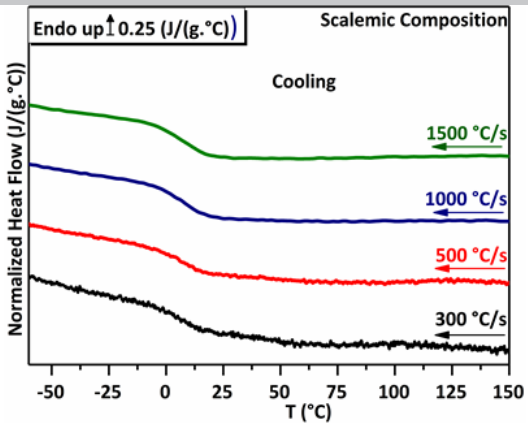

a)

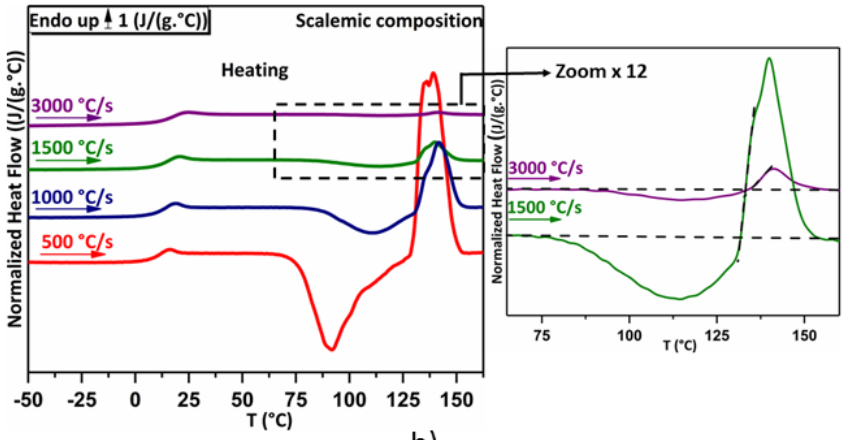

b)

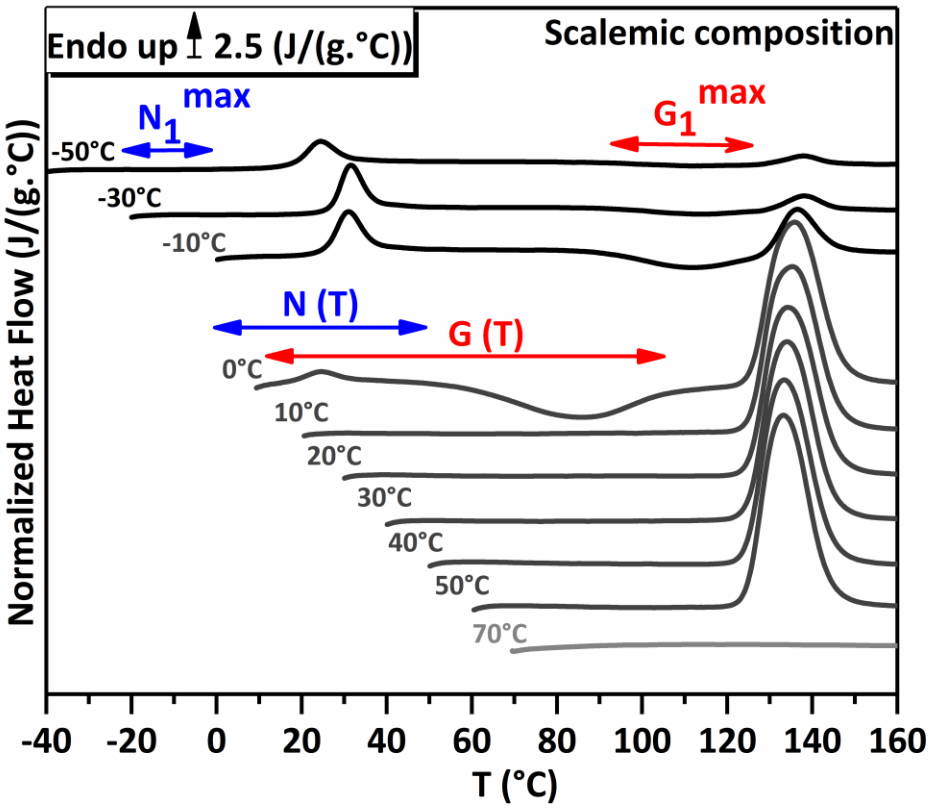
Endo up 2.5 (J/(g.°C))
Scalemic composition
N1 max
G1 max
-50°C
-30°C
-10°C
N (T)
G (T)
0°C
10°C
20°C
30°C
40°C
50°C
70°C
Normalized Heat Flow (J/(g.°C))
-40 -20 0 20 40 60 80 100 120 140 160
T (°C)